Identification and characterization of amphibian SLC26A5 using RNA-Seq

Zhongying Wang
Shanghai Jiao Tong University School of Medicine https://orcid.org/0000-0002-1752-4017
Qixuan Wang
Shanghai Jiao Tong University School of Medicine
Hao Wu
Shanghai Jiao Tong University School of Medicine
Zhiwu Huang (huangzw86@126.com)
Shanghai Jiao Tong University School of Medicine https://orcid.org/0000-0001-8802-8566

Research article

Keywords: RNA-Seq, SLC26A5, prestin, amphibian hearing organ, non-linear capacitance (NLC), 3D protein structure

Posted Date: December 2nd, 2020

DOI: https://doi.org/10.21203/rs.3.rs-118999/v1

Version of Record: A version of this preprint was published at BMC Genomics on July 22nd, 2021. See the published version at https://doi.org/10.1186/s12864-021-07798-6.

Abstract

Background

Prestin (SLC26A5) is responsible for acute sensitivity and frequency selectivity in the vertebrate auditory system. Due to lacking of the 3D structure, most of the mechanism of prestin is from experiments using site-directed mutagenesis or domain-swapping techniques after the amino acid residues were identified by comparing the sequence of prestin to those of its paralogs and orthologs. Frog prestin is the only representative in amphibian lineage. The knowledge of frog SLC26A5 is quite limited with only one species has been identified.

Results

Here we report a new coding sequence of SLC26A5 for a frog species, the American bullfrog (*Rana catesbeiana*). In our study, the SLC26A5 gene of bullfrog has been mapped, sequenced and cloned successively using RNA-SEq. The comparative study revealed an alignment with nearly 40% identity among bullfrogs and mammalian species. The predicted 3D protein structure showed that the frog prestin possessed a transmembrane domain (TM) and a STAS domain similar to the mammalian prestin. The function of prestin crucially relies on its integration into the cell membrane. Such localization was observed when a prestin-EGFP fusion protein was expressed in HEK293T cells. We measured the nonlinear capacitance (NLC) of prestin both in the hair cells of frog's inner ear and HEK293T cells transfected with this new coding gene. We observed that HEK293T cells expressing frog prestin showed electrophysiological features similar to that of hair cells from the amphibian's inner ear.

Conclusions

We mapped and sequenced the SLC26A5 of the American bullfrog from its inner ear cDNA using RNA-SEq. The frog SLC26A5 cDNA was 2,292 bp long, encoding a polypeptide of 763 amino acid residues, with 40% identity to mammals. After isolating the prestin gene of the frog, we generated a stable cell line transfected with this new coding gene and found it possessing similar electrophysiological features as the hair cells from the frog's auditory organ. Our experiment demonstrated that the new coding gene could encode a functionally active protein conferring NLC to both frog HCs and the mammalian cell line.

Background

Prestin is localized in the lateral wall of outer hair cells (OHCs), and is a membrane-based motor protein that powers electromotility, a central mechanism in the mammalian inner ear [1]. Electromotility is unique to OHCs, but absent in inner hair cells (IHCs). This mechanical activity is believed to feed back into the vibration of the cochlear partition, thereby enhancing the mechanical stimulus of IHCs [2]. SLC26A5 inactivation in mammals resulted in a loss of OHC somatic motility in vitro and a 40–60 dB loss of

cochlear sensitivity in vivo [1]. OHC electromotility has several salient features, and obtains its energy supply via changing membrane potential instead of ATP hydrolysis. Also, although internal Ca^{2+} levels modulate motility, the ions themselves do not participate in this activity. Moreover, this electromotility works in a cycle-by-cycle mode up to a frequency of at least 70 kHz, which is faster than any other biological force-generator [3, 4].

Prestin belongs to a large SLC26 (transporter family and constitutes a relatively novel group of protein known as the sulfate permease family, whose members are present in bacteria, fungi, plants, and animals [5]. Amino acid sequence analyses have identified prestin as the fifth member (SLC26A5) of this distinct anion transporter family. Although most members transport different anion substrates across the epithelia, prestin is unique, functioning as a voltage-dependent motor protein. Prestin is composed of a transmembrane domain, as well as of a carboxy-terminal sulfate transporter and anti-sigma factor antagonist (STAS) domain [6]. The STAS domain is critical for intracellular trafficking and protein-protein interactions [7]. OHC electromotility is accompanied by charge movement, which is characterized by a bell-shaped nonlinear capacitance (NLC) [2, 8]. NLC is regarded as the electrical signature of electromotility, which provides an intuitive readout of OHC function.

The unavailability of a prestin 3D structure signifies that most of our understanding of its mechanism is derived from experiments that use site-directed mutagenesis or domain-swapping techniques, after the amino acid residues were identified by comparing the prestin sequence to those of its paralogs and orthologs. Genome cloning of a wide range of species deduced the SLC26A5 amino acid sequences of more than 45 species [9–12]. Frog prestin is the only representative amphibian lineage. The only study on frog prestin describes the sequenced genomes of *Xenopus tropicalis* (xPres) [13]. The present study aimed to map and sequence the *SLC26A5* gene from a new frog species, the American bullfrog (*Rana catesbeiana*; rPres) via RNA sequencing (RNA-Seq), using cDNA from the frog's inner ear. The high-throughput RNA-Seq technique, based on next-generation sequencing technology, has emerged as a useful tool for transcriptome analysis and for exploring unknown genes. RNA-Seq provides a significantly more precise measurement of transcripts than other methods and has been successfully used for gene discovery in various species [14, 15]. In order to determine if this new sequenced gene could encode a functionally active protein, we generated a stable cell line that expressed frog prestin. Using the whole-cell patch-clamp method, we observed that HEK293T cells expressing frog prestin showed electrophysiology similar to that of hair cells from the amphibian's inner ear.

Results

rPres gene identification

Inner ear tissues of 10 frogs were enough for a cDNA library to be constructed and sequenced. In total, 94,937,050 reads were obtained from the library. Quality controls performed to ensure the reliability of the library generated 92,356,656 clean reads for mapping. Using the Hisat software, 70.9% clean reads were mapped to the genome, among which more than 93.02% had quality scores at a ratio of Q30 (base

quality > 30 and error rate < 0.001). Gene annotation was performed via BLAST searches (E-value ≤ 10 − 5) against the Nr (NCBI non-redundant protein sequences), Nt (NCBI nucleotide sequences), and Pfam (protein family) databases.

Analyses of prestin orthologs

We obtained the prestin coding regions of gerbil (*Meriones unguiculatus*), tropical clawed frog (*Xenopus tropicalis*), and chicken (*Gallus gallus*) using BLAST analysis of the Ensembl and NCBI genomic databases. TBlastN was employed to search for prestin sequences in the genome databases of the American bullfrog (*Rana catesbeiana*) using known prestin protein sequences. BLAST analysis of putative gene sequences through GenBank ensured that the best hits corresponded to known prestin genes. Using the CLUSTAL method, alignment of the online gerbil prestin gene and the full-length bullfrog prestin sequence mapped by RNA-Seq were conducted (Fig. 2), revealing an alignment with nearly 40% identity among bullfrogs and mammalian species.

Heterologously-expressed frog prestin is localized in the cell membrane

The function of prestin crucially relies on its integration into the cell membrane. Such localization was observed when an rprestin-EGFP fusion protein was expressed in HEK293T cells. Membrane expression of the protein was examined using confocal microscopy (Fig. 1B). From the predicted 3D protein structure, it was clear that the frog prestin possesses a transmembrane domain (TM) and a STAS domain similar to the mammalian prestin (Fig. 1C). The TM domain has two subdomains: a compact core domain that holds the substrate binding site and a gate domain that shields one side of the core domain. The STAS domain was relevant for intracellular trafficking and protein-protein interactions (Fig. 1C). Changes in transmembrane electrical potential induced charge displacement in prestin.

rPres confers NLC to HEK293T cells

The voltage-clamped frog hair cell was depolarized from a holding potential of − 80 mV to − 20 mV. During the depolarizing stimulus, the Ca^{2+} current was recorded (Fig. 3A). Voltage steps (300 ms in duration) varying from − 150 to 100 mV, in 10 mV steps, were used for NLC recordings after the Ca^{2+} current was blocked by Cd^{2+} at a concentration of 0.4 mM (Fig. 3B). NLC from HCs and transfected cells was measured using a voltage stimulus consisting of a sine wave superimposed onto a voltage ramp. Using the first derivative of the Boltzmann function, four parameters (Q_{max}, C_{lin}, $V_{1/2}$, and z) from nonlinear curve-fitting of the NLC were calculated. HEK293T cells varied in size, which is correlated to the C_{lin} value. We therefore normalized Q_{max} to C_{lin} in order to compare the magnitude of the charge movement measured from cells of different sizes.

NLC measurements were analyzed from eight frog HCs (Fig. 3C)and eight rPres-transfected HEK293T cells (Fig. 3D). The mean and SD values of rPres were: Q_{max} = 1.5 ± 0.7 (fC), Q_{max}/C_{lin} = 0.15 ± 0.07

(fC/pF), $V_{1/2}$ = − 31.1 ± 8.1 (mV), z = 2.8 ± 0.8. The mean and SD values of frog HCs were: Q_{max} = 11.1 ± 7.7 (fC), Q_{max}/C_{lin} = 0.79 ± 0.4 (fC/pF), $V_{1/2}$ = − 15 ± 4 (mV), z = 2.9 ± 0.6. The charge density of rPres NLC recorded from HEK293T cells was less than that from frog HCs (Fig. 4A, B; P < 0.01, Student's *t*-test). Another notable functional parameter was $V_{1/2}$ (Fig. 4C), which was significantly more hyperpolarized in rPres-transfected cells than in frog hair cells. Moreover, no significant difference was observed in the z value between the two cell types (Fig. 4D). We detected no NLC in cells transfected with the EGFP-vector only (Fig. 5D).

NLC was also measured from two other species, Xenopus (xPres) and chicken (cPres) (Fig. 5B, C). Interestingly, both amphibian species generated NLC curves. The rPres charge density was considerably less than that of xPres (Fig. 6A, B; P < 0.01, Student's *t*-test), while $V_{1/2}$ and z values varied markedly between the two (Fig. 6C, D; P < 0.01, Student's *t*-test). NLC was undetected in cells transfected with cPres (Fig. 5C). All the data are shown in Table 1.

Discussion

Brownell discovered that mammalian OHCs were able to alter their length when electrically stimulated [16]. Following the discovery of "electromotility", the study of its mechanism and role in the vertebrate auditory system became one of the most exciting areas in hearing research. Experiments which detected cellular motility even after the degradation of the cell's content via internal tryptic digestion suggested that a molecular motor in the plasma membrane drives the mechanism of force generation [17]. The surface area of the plasma membrane was covered to nearly 70% by prestin. OHCs demonstrate piezoelectric properties with an efficiency of conversion from mechanical force to electrical charge is approximately four times greater than that of the best man-made piezoelectric material [18].

Prestin typically shares the protein structure of the SLC26A family: a conserved central region of hydrophobic amino acids with N- and C-terminal residues on the cytoplasmic side of the plasma membrane. The sulfate transporter (SulTP) sequence is located in the hydrophobic core, while a STAS domain with clusters of charged residues is present in the C-terminal region. Amino acids in the SulTP domain are almost identical among mammalian species, such as humans, mice, rats, and gerbils [19]. Although prestin was identified 20 years ago, its experimental 3D structure is still unavailable. Prestin may contain specific domains that serve as the 'voltage sensor' (to detect voltage change) and the 'actuator' (to generate length change and force). Their fundamental characteristics and mechanisms, however, remain unexplored. Approximately 200 amino acid residues have since been mutated, to determine the mechanism of action in the voltage sensor and identify sequences critical for prestin function [20]. Another approach to probe the region responsible for motor capability involves locating residues that are conserved in mammalian prestin, but variable in non-mammalian prestin orthologs. To further understand the molecular and cellular mechanisms underlying this mysterious motor protein, we attempted the mapping, sequencing, and cloning of a non-mammalian prestin ortholog using RNA-Seq.

The bullfrog SLC26A5 cDNA is 2,292 bp long, and encodes a predicted polypeptide of 763 amino acid residues. After isolating the prestin gene from the inner ear cDNA of the American bullfrog, we generated a stable cell line transfected with this new coding gene. Confocal images localized the heterologously-expressed frog prestin in the plasma membrane (Fig. 1B). NLC was measured both in HCs from the frog's inner ear (Fig. 3A–C), and in HEK293T cells expressing frog prestin, to analyze its functional property (Fig. 3D). For each cell type, four parameters (Q_{max}, C_{lin}, $V_{1/2}$, and z) of NLC were calculated. The charge density in frog HCs was higher than that recorded in HEK293T cells (Fig. 4A, B). Based on the fundamental assumption that a direct relationship exists between the molecular density of the protein in the cell membrane and the amount of charge recorded by the electrode [21], it is reasonable to conclude from our results that the density of endogenously-expressed prestin is higher than when expressed in the cell line. The z values obtained here should be noted (Fig. 4D). The absence of a significant difference in the z value between the two cell types suggests that the same charge is moving through the transmembrane electrical field within the protein. Alterations in intracellular ion concentration can shift the $V_{1/2}$ direction within a range of − 180 and greater than 100 mV [22]. We observed a shift in $V_{1/2}$ to a more positive direction from the frog AP cells, due to variations in intracellular conditions between these and HEK293T cells (Fig. 4C). Our experiment demonstrated that the new coding gene could encode a functionally active protein conferring NLC to both frog HCs and the mammalian cell line. As previous studies have shown that non-mammalian prestin does not demonstrate motor capability, and that the motor function of prestin is a newly derived molecular property exclusive to mammals [9, 13, 23], we did not attempt to examine the motor capability of frog prestin in the present study. The lack of motor function in non-mammalian prestin indicates that the 'voltage sensor' and 'actuator' in the molecule may evolve independently and have different structural bases.

Analysis of the gerbil and bullfrog prestin amino acid sequences revealed approximately 40% identity among the two species (Fig. 1). Pendrin, the closest mammalian prestin paralog, carries 40% sequence identity and exhibits no voltage-dependent NLC [24]. Zebrafish prestin carries more than 50% sequence identity compared to that of mammals, and possesses no electrophysiological characteristics. As the voltage sensing range of zebrafish prestin is not within the range of − 150 mV to 100 mV, uncertainty remains as to whether a two-state Boltzmann function is appropriate for its description [23]. Studies on avian species revealed that two types of HCs occur in the chick inner ear, neither of which possess voltage-dependent non-linear capacitance [9]. However, contrasting results from immunolabeling studies by Maryline Beurg confirmed the presence of chicken prestin in the hair cell lateral membrane, and demonstrated that HCs of the chicken auditory papilla possessed NLC [25]. NLC from cPres-expressing cell lines was not measured in the present study (Fig. 5C). Previous studies focusing on amphibian prestin are quite rare, thereby limiting knowledge of its function. NLC measurements from xPres-expressing cell lines revealed that xPres possessed similar electrophysiological features as rPres (Fig. 6). If the functional evolution of prestin is characterized by a gradual gain of NLC as demonstrated in a previous study, frog prestin would therefore be evolutionarily more advanced than avian and teleost prestin [11, 13]. The presence of NLC in frog prestin might suggest a common mechanism within the protein structure for their functional significance both in mammalian and amphibian prestin. The

predicted 3D structure of gerbil and frog prestin showed that they shared a similar framework (Fig. 2C). It is reasonable to assume that the voltage sensor of prestin consisted of residues present in the frog prestin sequence, but absent in pendrin and chick prestin. Further comparative studies may reveal the molecular peculiarities underlying the mechanisms of prestin.

Conclusion

Because data on the amphibian SLC26A5 gene is limited, we mapped and sequenced that of the American bullfrog from its inner ear cDNA using RNA-SEq. The frog SLC26A5 cDNA is 2,292 bp long, encoding a polypeptide of 763 amino acid residues, with 40% identity to mammals. We generated a stable cell line expressing frog prestin, which possessed similar electrophysiological features as the HCs from the frog's auditory organ. The present study explored non-traditional species sequence information to increase our knowledge of the mechanisms involved in prestin function.

Methods

Animals

About 20 healthy adult American bullfrogs (*Rana catesbeiana*) were obtained from the same supplier (Qingpu bullfrog farm, Shanghai). Care and use of animals were conducted in accordance with the Guide for the Care and Use of Laboratory Animals (National Institutes of Health, USA) and approved by the University Committee of Laboratory Animals, Shanghai Jiao Tong University.

10 bullfrogs weighted about 1.5 kg were sedated in an ice bath for 20 min, double-pithed, and decapitated. Inner ears of the bullfrogs were dissected and immediately immersed in RNAlater, for subsequent mRNA isolation.

RNA isolation, library construction, and sequencing

Total RNA was isolated from the bullfrog's inner ear using TRIzol reagent (Invitrogen, CA, USA) according to the manufacturer's instructions. RNA quality and concentration were determined using 1.2% agarose gels and an Agilent 2100 Bioanalyzer system (Agilent Technologies, CA, USA). RNA degradation was determined using 1.2% agarose gels. RNA concentration and purity levels were measured using a NanoDrop 2000 spectrophotometer (Thermo Scientific, MA, USA). Its integrity was confirmed using an Agilent Bioanalyzer 2100 system. Sequencing libraries were generated using a NEBNext® Ultra™ RNA Library Prep Kit for Illumina® (NEB, MA, USA). mRNA was purified from 3 μg of RNA using oligo (dT) magnetic beads, and was randomly sheared into pieces of approximately 200 base pairs in the fragmentation buffer. Fragmented mRNAs were then used for first-strand cDNA synthesis using reverse transcriptase and random hexamer primers. The second-strand cDNA was synthesized using DNA polymerase I and RNase H. Following fragment ligatation to adapters, polymerase chain reaction (PCR) was used to isolate the adapter-modified fragments. The generated libraries were assessed for quality using an Agilent 2100 Bioanalyzer and a real-time PCR system, and were sequenced using an Illumina

HiSeq 2500 platform (Illumina, CA, USA). Trinity (version: v2.8.4) software was used for the de novo assembly of unmapped reads, which has been efficient for the de novo reconstruction of transcriptomes from RNA-Seq data.

Generation of stable cell lines that express rPres

CRISPR/Cas9-mediated gene editing was used for AAVS1 site-specific integration. The donor vector was designed to express rPres-EGFP fusion proteins (Fig. 1A). The HEK293T cell line (RRID:CVCL_0063) was kindly provided by the institute of neuroscience (Chinese Academy of Sciences). Cells were cultured in Dulbecco's modified Eagle's medium (DMEM) (Invitrogen, Carlsbad, CA, USA) supplemented with 10% fetal bovine serum (FBS) (Invitrogen). HEK293T cells were co-transfected with the sgRNA/Cas9 and donor plasmids. Puromycin was added to the culture medium 24 h after transfection, for screening purposes. Cells transfected with the EGFP-vector were used as a negative control.

Confocal imaging

The stable cell line was cultured for 12 h before scanned. Cells were first rinsed with phosphate-buffered saline (PBS), then fixed and permeabilized with 4% paraformaldehyde and 1% Triton X-100 for 30 min. The cells were then washed twice, each for 15 min. Confocal images were captured using a laser scanning microscope (Leica Microsystems, Germany) using a 63 × oil immersion objective (Fig. 1B).

Electrophysiology

Recordings of hair cells (HCs) from another 10 frogs were performed at 22 °C, within 2 h of dissection. Patch pipettes were of thick-walled borosilicate glass (World Precision Instruments) with a Narishige puller (model PP-830), pulled to a resistance of approximately 6 MΩ, and coated with dental wax. NLC was measured by recording dissected amphibian papillae (AP) in an extracellular solution containing (in mM): 95 NaCl, 2KCl, 1 $MgCl_2$, 10 TEA-Cl, 2 $CaCl_2$, 3Glucose, 1creatine,1pyruvate and 10 HEPES at pH 7.30 (240 mOsmol L^{-1}). NaOH was used for pH adjustment. The internal solution for the HCs contains (in mM) : 80Cs-gluconate□20CsCl□10HEPES□2EGTA□3 Mg-ATP□0.5Na-GTP□10TEA-Cl (pH 7.30; 240 mOsmol L^{-1}). CsOH was used for pH adjustment. Whole-cell voltage-clamp recordings were obtained using an EPC-10/2 (HEKA Electronics) patch-clamp amplifier and the Pulse software (HEKA). The HCs were maintained at − 80 mV, and off-line analysis was primarily using the Igor Pro 5.0 software (Wavemetrics).

HEK293T cells were detached and then bathed in an extracellular solution containing (in mM): 120 NaCl, 20 TEA-Cl, 2 $CoCl_2$, 2 $MgCl_2$, 10 HEPES, 5 glucose (pH 7.2). Osmolarity was adjusted to 300 mOsmol L^{-1} with glucose. Patch pipettes were pulled to resistances of 4–6 MΩ and coated with dental wax. The internal solution was (in mM): 140 CsCl, 2 $MgCl_2$, 10 EGTA and 10 HEPES. NLC measurements were performed on cultured cells with stable membrane-associated EGFP expression. After rupture, we selected cells whose membrane resistance was over 600 MΩ and showed normal Cm and Rm values. Whole-cell voltage-clamp recordings were obtained using an EPC-10/2 (HEKA Electronics) patch-clamp amplifier and the Pulse software (HEKA). The cells were maintained at − 80 mV. Off-line analysis was performed mainly using the Igor Pro 5.0 software (Wavemetrics).

The sine + DC software lock-in function of Patchmaster was used to obtain voltage-dependent currents and capacitance; a voltage protocol was designed including both ramp and sine stimulation (800 Hz with a 10-mV amplitude). Sine waves were superimposed onto ramps from − 150 mV to 100 mV for a duration of 300 ms. The NLC was fitted with the derivative of a Boltzmann function:

$$Cm = \frac{Q_{max}\alpha}{exp\left[\alpha\left(V_m - V_{\frac{1}{2}}\right)\right]\left(1 + exp\left[-\alpha\left(V_m - V_{\frac{1}{2}}\right)\right]\right)^2} + C_{lin}$$

where Q_{max} was the maximum charge transfer, $V_{1/2}$ referred to the voltage at half-maximum charge transfer, C_{lin} represented the linear membrane capacitance, and α was the slope factor describing the voltage dependence. α = ze/kT, where k was Boltzmann's constant, T was the absolute temperature, z was the valence of charge movement, and e was the electron charge.

Data Analysis and Statistical Tests

Data were analyzed in Igor Pro (WaveMetrics, USA) with home-made macros and statistical tests were performed in Prism (GraphPad, USA) with built-in functions. Depending on the nature of data set, statistical significance was assessed with unpaired Student's t-test. Data are presented as Mean ± SD, and the level of significance was set to $p < 0.05$. In figures, ∗ means $p < 0.05$, ∗∗ means $p < 0.01$.

Abbreviations

SLC26: solute carrier family 26; NLC:nonlinear capacitance; OHC:outer hair cells; IHC:inner hair cells; SulP:sulfate permease; STAS:sulfate transporter and anti-sigma factor antagonist; TM:transmembrane

Declarations

Acknowledgements

We thank professor Lei Song for technical support in electrophysiology. Thank professor Chenhui Huang for the comment in our RNA-seq experiment. Thank professor Dehong Yu for her suggestions in our cell line study.

Author Contributions

ZW conceived the reported study and performed the experiments. QW performed the experiments and undertook data analyses. The manuscript was primarily written by ZW, but with contributions from ZH and HW, and then reviewed by all the authors. All authors have read and agreed to the published version of the manuscript.

Funding

This work was funded by the National Natural Science Foundation of China (NSFC) to H.W. (81730028) and the Shanghai Key Laboratory of Translational Medicine on Ear and Nose Diseases (14DZ2260300).

Availability of data and materials

The genome sequences of gerbil (*Meriones unguiculatus*), tropical clawed frog (*Xenopus tropicalis*), and chicken (*Gallus gallus*) could be accessed at GenBank under the accessions 110554811, 100497573, and 417715, respectively.

Ethics approval and consent to participate

All animals used in the current study were approved by the Institutional Animal Care and Use Committee in Shanghai Ninth People's Hospital, School of medicine, Shanghai Jiao Tong University. Written nformed consent to participate was obtained from the farm owners.

Consent for publication

Not applicable.

Competing interests

The authors declare that they have no competing interests.

Author details

[1]Department of Otolaryngology-Head and Neck Surgery, Shanghai Ninth People's Hospital, Shanghai Jiao Tong University School of Medicine, Shanghai, China; Ear Institute, Shanghai Jiao Tong University School of Medicine, Shanghai, China; Shanghai Key Laboratory of Translational Medicine on Ear and Nose Diseases, Shanghai, China.

References

1. Liberman MC, et al. Prestin is required for electromotility of the outer hair cell and for the cochlear amplifier. Nature. 2002;419(6904):300–4.
2. Zhai F, et al. Maturation of Voltage-induced Shifts in SLC26a5 (Prestin) Operating Point during Trafficking and Membrane Insertion. Neuroscience. 2020;431:128–33.
3. Kachar B, et al. Electrokinetic shape changes of cochlear outer hair cells. Nature. 1986;322(6077):365–8.
4. Frank G, Hemmert W, Gummer AW. Limiting dynamics of high-frequency electromechanical transduction of outer hair cells. Proc Natl Acad Sci U S A. 1999;96(8):4420–5.
5. Kuwabara MF, et al. The extracellular loop of pendrin and prestin modulates their voltage-sensing property. J Biol Chem. 2018;293(26):9970–80.

6. Chang YN, et al., *Structural basis for functional interactions in dimers of SLC26 transporters.* Nat Commun, 2019. **10**(1): p. 2032.
7. Shibagaki N, Grossman AR. The role of the STAS domain in the function and biogenesis of a sulfate transporter as probed by random mutagenesis. J Biol Chem. 2006;281(32):22964–73.
8. Oliver D, et al. Intracellular anions as the voltage sensor of prestin, the outer hair cell motor protein. Science. 2001;292(5525):2340–3.
9. He DZ, et al. Chick hair cells do not exhibit voltage-dependent somatic motility. J Physiol. 2003;546(Pt 2):511–20.
10. Santos-Sacchi J, Tan W. The Frequency Response of Outer Hair Cell Voltage-Dependent Motility Is Limited by Kinetics of Prestin. J Neurosci. 2018;38(24):5495–506.
11. Tan X, et al. From zebrafish to mammal: functional evolution of prestin, the motor protein of cochlear outer hair cells. J Neurophysiol. 2011;105(1):36–44.
12. Weber T, et al. Expression of prestin-homologous solute carrier (SLC26) in auditory organs of nonmammalian vertebrates and insects. Proc Natl Acad Sci U S A. 2003;100(13):7690–5.
13. Tang J, et al. Lizard and frog prestin: evolutionary insight into functional changes. PLoS One. 2013;8(1):e54388.
14. Monger C, et al. A Bioinformatics Pipeline for the Identification of CHO Cell Differential Gene Expression from RNA-Seq Data. Methods Mol Biol. 2017;1603:169–86.
15. Patrick R, et al. Sierra: discovery of differential transcript usage from polyA-captured single-cell RNA-seq data. Genome Biol. 2020;21(1):167.
16. Brownell WE, et al. Evoked mechanical responses of isolated cochlear outer hair cells. Science. 1985;227(4683):194–6.
17. Kalinec F, et al. A membrane-based force generation mechanism in auditory sensory cells. Proc Natl Acad Sci U S A. 1992;89(18):8671–5.
18. Dong XX, Ospeck M, Iwasa KH. Piezoelectric reciprocal relationship of the membrane motor in the cochlear outer hair cell. Biophys J. 2002;82(3):1254–9.
19. Okoruwa OE, et al. Evolutionary insights into the unique electromotility motor of mammalian outer hair cells. Evol Dev. 2008;10(3):300–15.
20. He DZ, et al. Tuning in to the amazing outer hair cell: membrane wizardry with a twist and shout. J Membr Biol. 2006;209(2–3):119–34.
21. Seymour ML, et al. Membrane prestin expression correlates with the magnitude of prestin-associated charge movement. Hear Res. 2016;339:50–9.
22. Song L, Seeger A, Santos-Sacchi J. On membrane motor activity and chloride flux in the outer hair cell: lessons learned from the environmental toxin tributyltin. Biophys J. 2005;88(3):2350–62.
23. Albert JT, et al. Voltage-sensitive prestin orthologue expressed in zebrafish hair cells. J Physiol. 2007;580(Pt. 2):451–61.

24. Tang J, et al. Engineered pendrin protein, an anion transporter and molecular motor. J Biol Chem. 2011;286(35):31014–21.
25. Beurg M, Tan X, Fettiplace R. A prestin motor in chicken auditory hair cells: active force generation in a nonmammalian species. Neuron. 2013;79(1):69–81.

Tables

	C_{lin} (pF)	Q_{max} (fC)	$V_{1/2}$ (mV)	z	Q_{max}/C_{lin} (fC/pF)
AP (n = 8)	11.2 ± 3	11.1 ± 7.7	-15 ± 4	2.9 ± 0.6	0.79 ± 0.4
rPres (n = 8)	9.7 ± 2	1.5 ± 0.7	-31.1 ± 8.1	2.8 ± 0.8	0.15 ± 0.07
xPres (n = 12)	13.5 ± 3.7	29.8 ± 25	60.5 ± 25	0.62 ± 0.14	2.38 ± 2

Table 1 All the measurements performed in the present study are expressed as mean ± sd.

Supplementary Information

All data generated or analysed during this study are included in this published article and its supplementary information files.

Figures

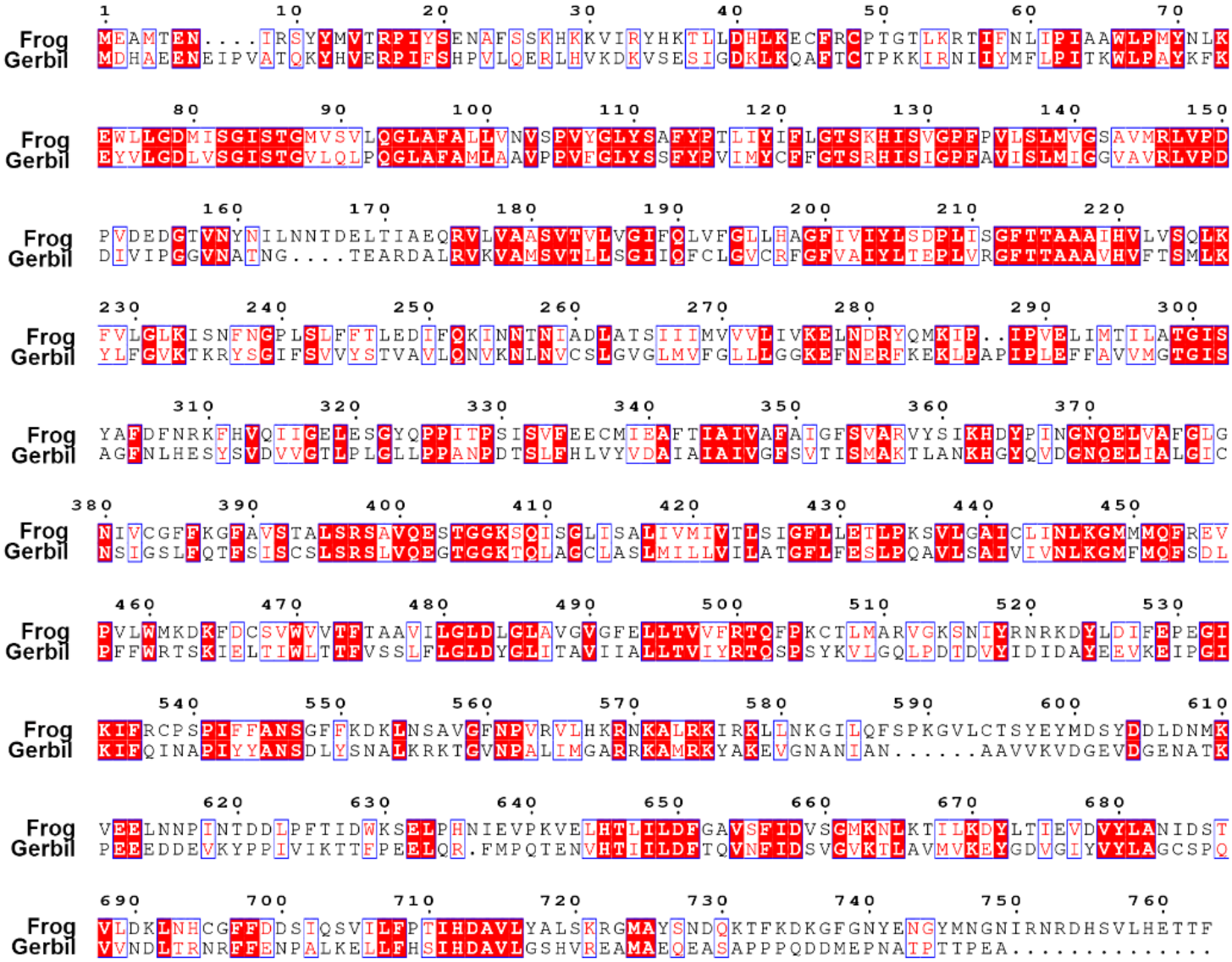

Figure 1

Alignment of amino acid sequences of frog and gerbil prestin. Different colors had been used to represent identity of each residue among two species. Red block: Full identity at a residue; red letter: Partial identity at a residue; Black: complete disparity at a residue. Gaps in the aligned sequences were indicated by the dashed line.

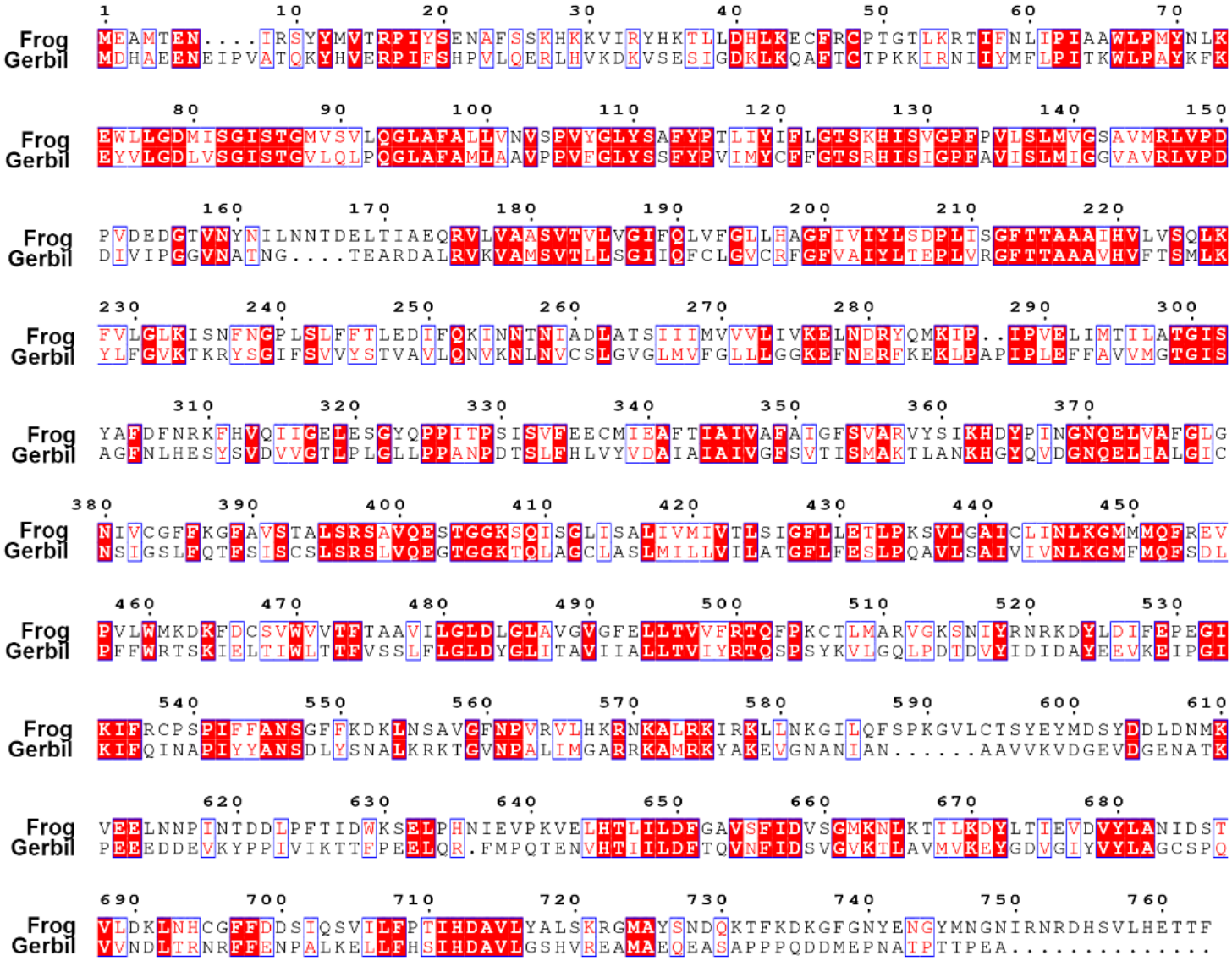

Figure 1

Alignment of amino acid sequences of frog and gerbil prestin. Different colors had been used to represent identity of each residue among two species. Red block: Full identity at a residue; red letter: Partial identity at a residue; Black: complete disparity at a residue. Gaps in the aligned sequences were indicated by the dashed line.

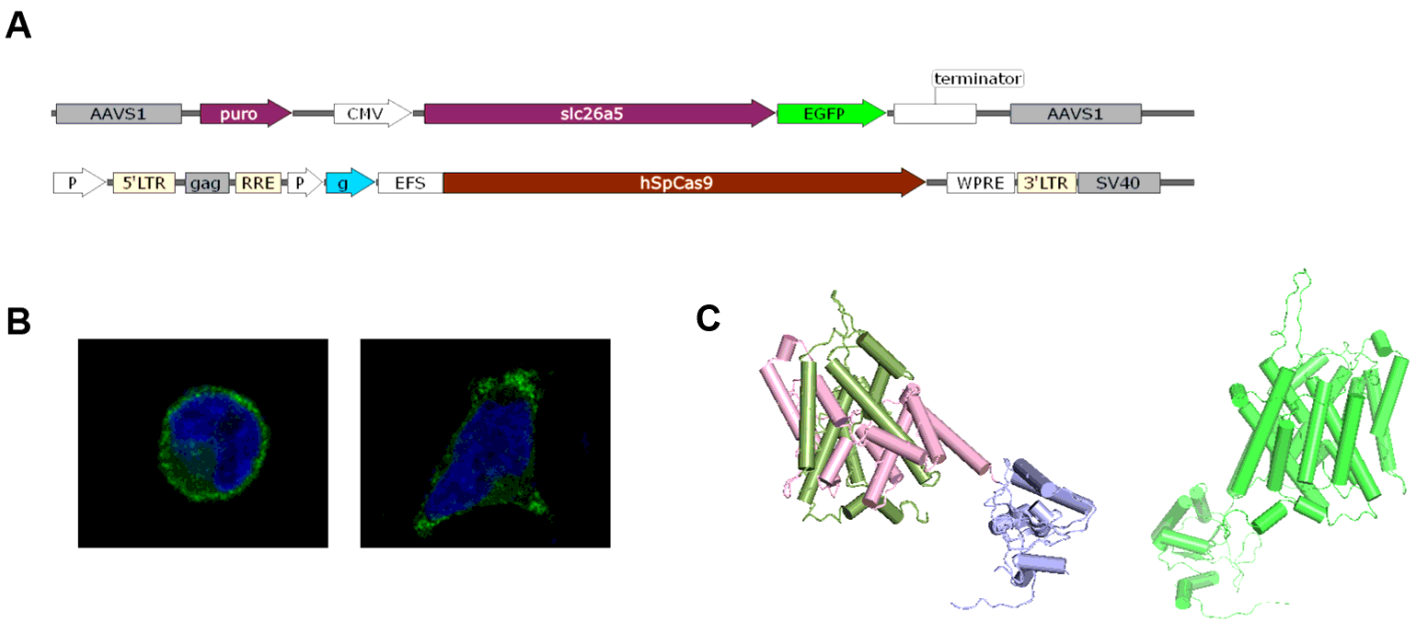

Figure 2

Frog prestin localized in the cell membrane. A), Donor vector designed for expression of fPres-EGFP fusion protein and CRISPR/Cas9-mediated gene editing vector. B), Membrane expression of fPres in HEK293T cells was examined using confocal microscopy. The left one was a detached cell and the right one was an attached cell. C), Predicted protein structure of frog prestin (left). The transmembrane domain holds two intertwined inverted repeats of seven TM segments. The N- and C-terminal halves of the TM domain are green and pink, respectively. The STAS domain is within the purple part. Predicted protein structure of gerbil prestin (right).

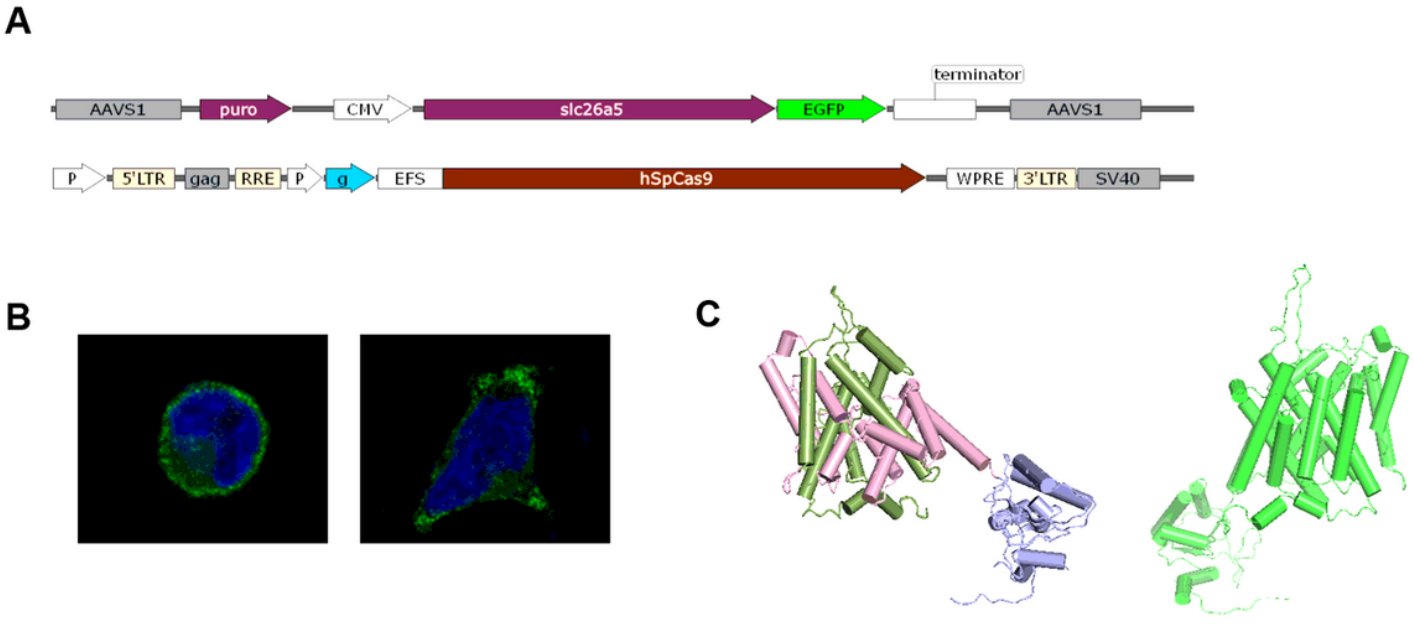

Figure 2

Frog prestin localized in the cell membrane. A), Donor vector designed for expression of fPres-EGFP fusion protein and CRISPR/Cas9-mediated gene editing vector. B), Membrane expression of fPres in HEK293T cells was examined using confocal microscopy. The left one was a detached cell and the right one was an attached cell. C), Predicted protein structure of frog prestin (left). The transmembrane domain holds two intertwined inverted repeats of seven TM segments. The N- and C-terminal halves of the TM domain are green and pink, respectively. The STAS domain is within the purple part. Predicted protein structure of gerbil prestin (right).

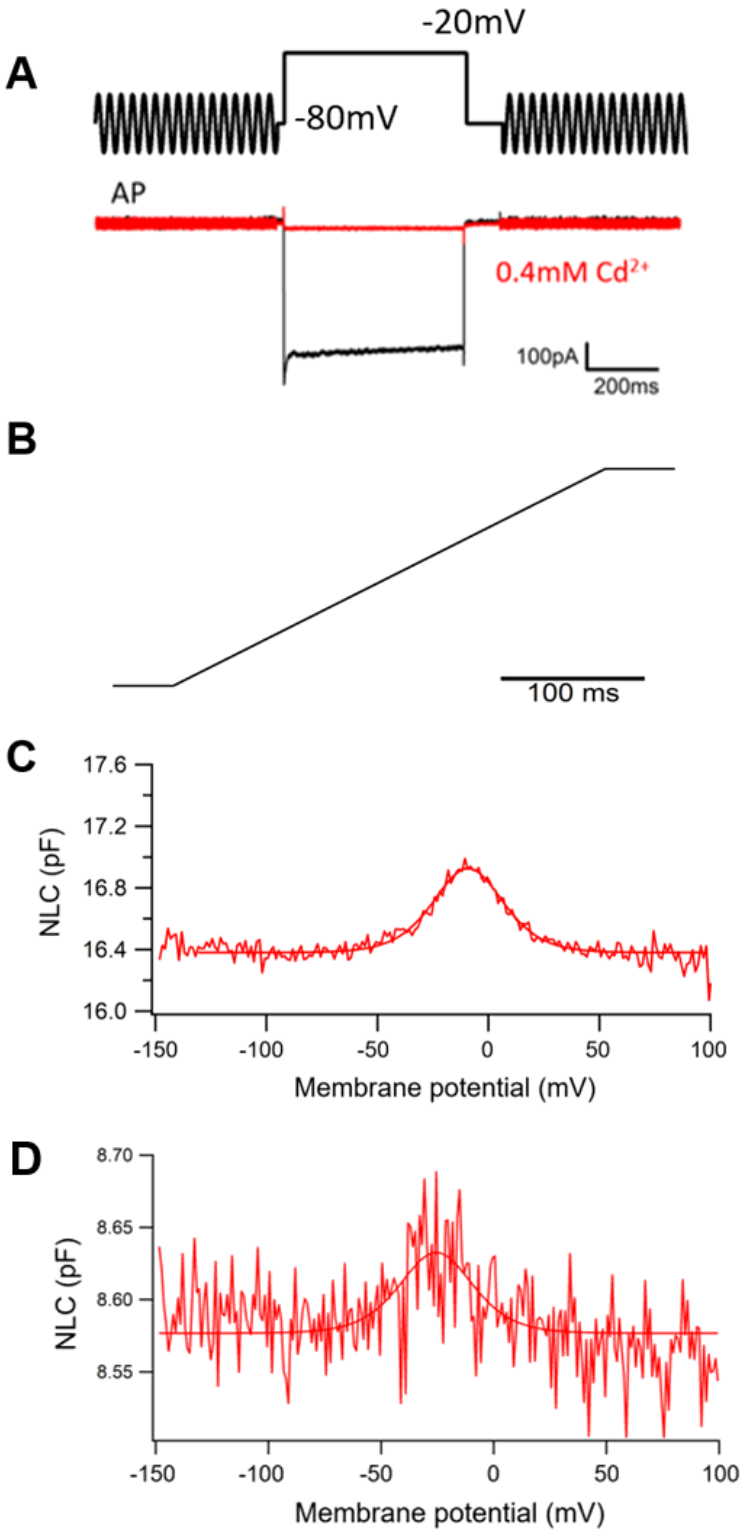

Figure 3

The nonlinear capacitance measurements in the hair cells from amphibian inner ear and exogenous expressed cells. A), The voltage-clamped frog hair cell was depolarized from a holding potential of -80mV to -20mV. During the depolarizing stimulus, a Ca2+ current was recorded. After the Ca2+ current was blocked by the Cd2+ at a concentration of 0.4mM. B), Voltage steps (300 ms in duration) varied from -150 to 100 mV in 10 mV steps were used for capacitance recordings. C), Non-linear capacitance obtained from the hair cells of AP and D), the rPres transfected cells.

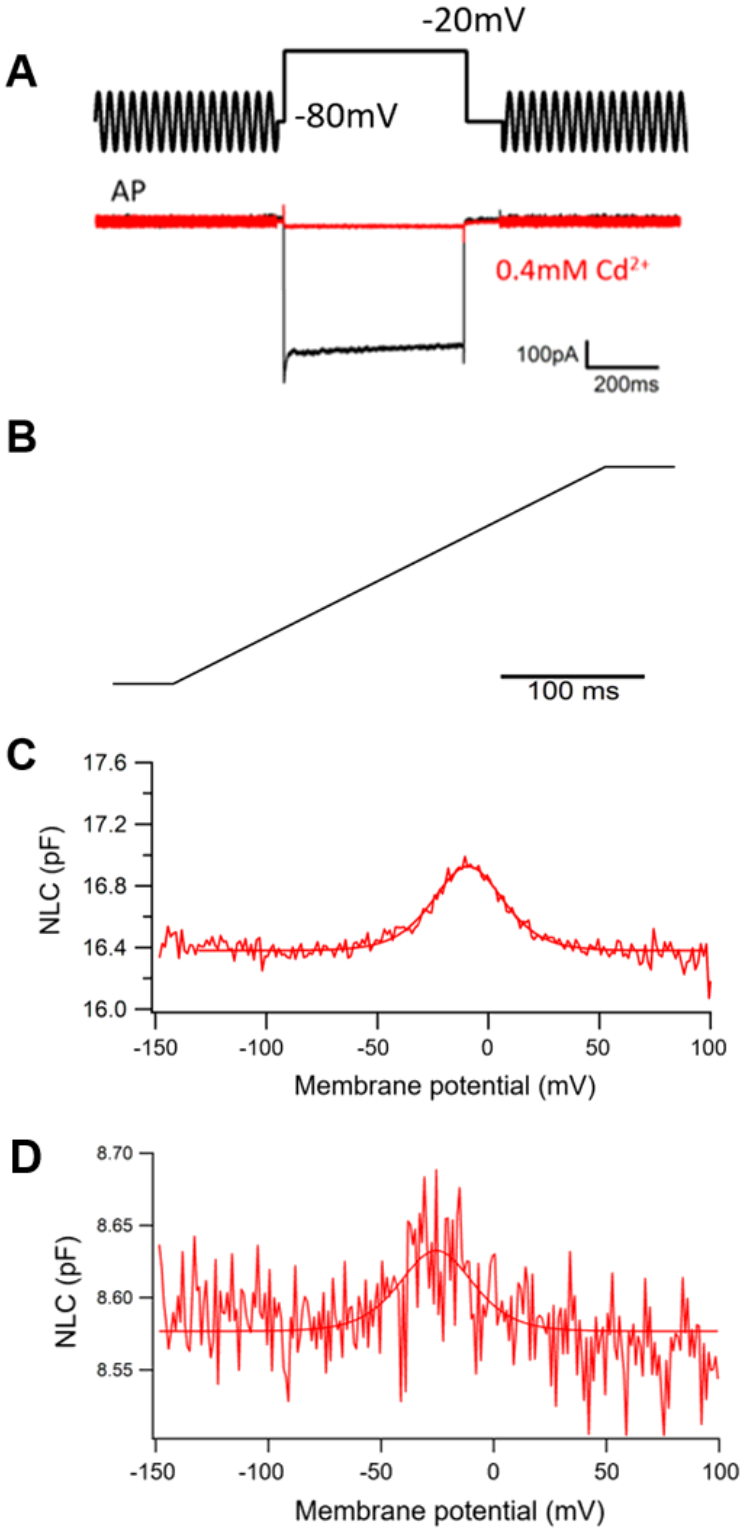

Figure 3

The nonlinear capacitance measurements in the hair cells from amphibian inner ear and exogenous expressed cells. A), The voltage-clamped frog hair cell was depolarized from a holding potential of -80mV to -20mV. During the depolarizing stimulus, a Ca2+ current was recorded. After the Ca2+ current was blocked by the Cd2+ at a concentration of 0.4mM. B), Voltage steps (300 ms in duration) varied from -150 to 100 mV in 10 mV steps were used for capacitance recordings. C), Non-linear capacitance obtained from the hair cells of AP and D), the rPres transfected cells.

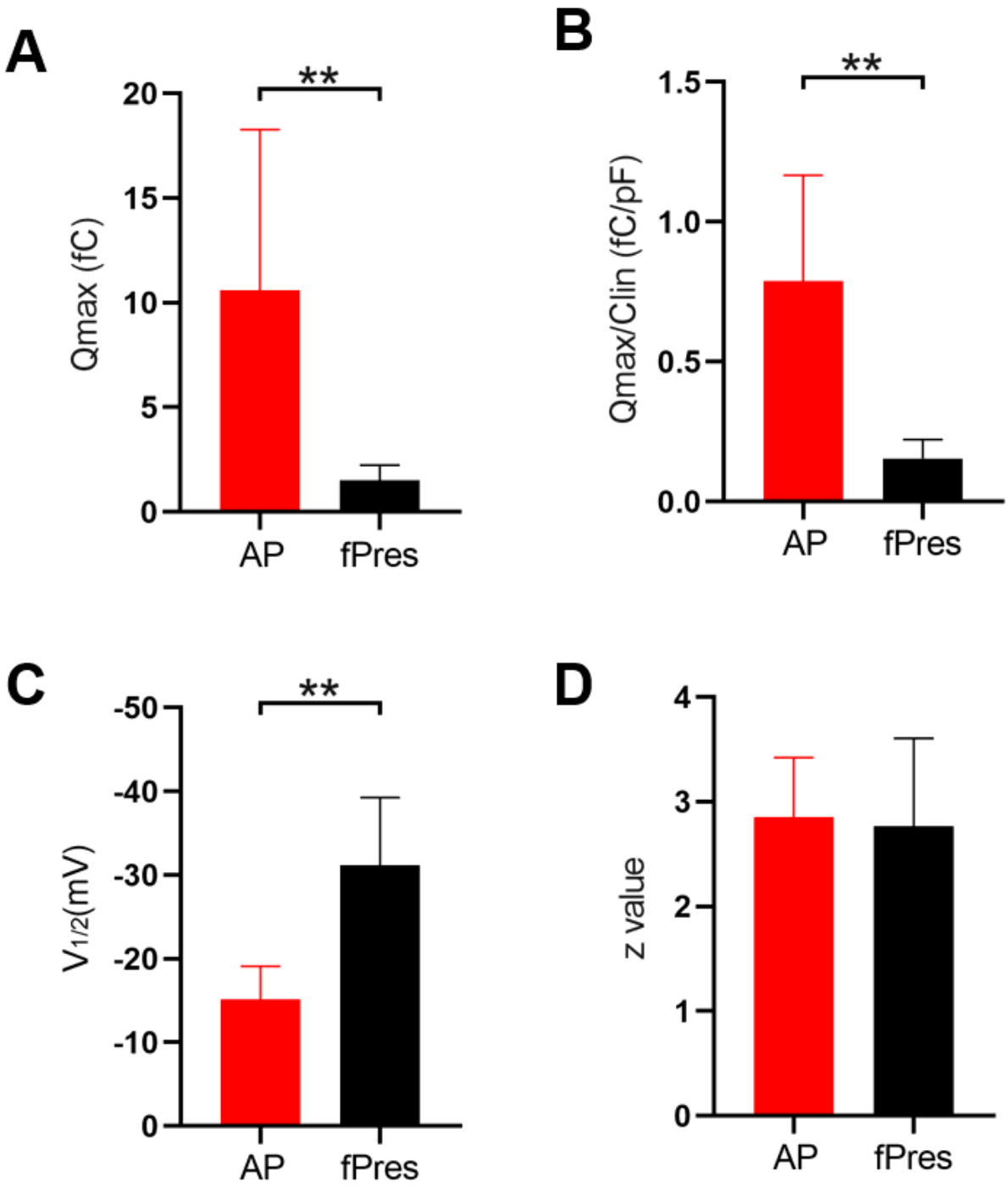

Figure 4

NLC datas of AP hair cells and fPres. A, B, C, D) Showed four parameters derived from curve fittings with Boltzmann's function for AP hair cells (n=8) and fPres (n=8). Datas were expressed as mean±s.d. *P < 0.05□**P < 0.01

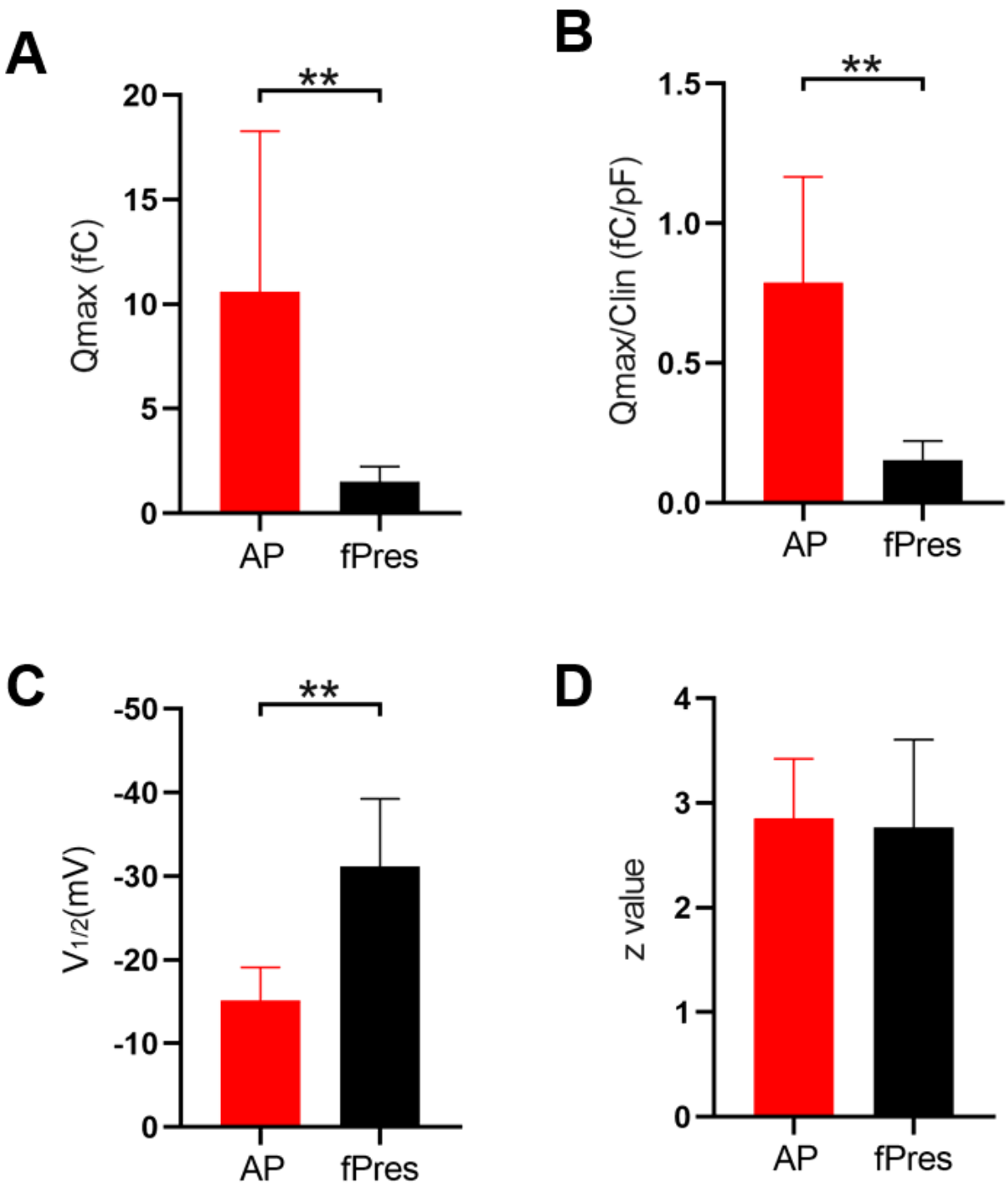

Figure 4

NLC datas of AP hair cells and fPres. A, B, C, D) Showed four parameters derived from curve fittings with Boltzmann's function for AP hair cells (n=8) and fPres (n=8). Datas were expressed as mean±s.d. *P < 0.05□**P < 0.01

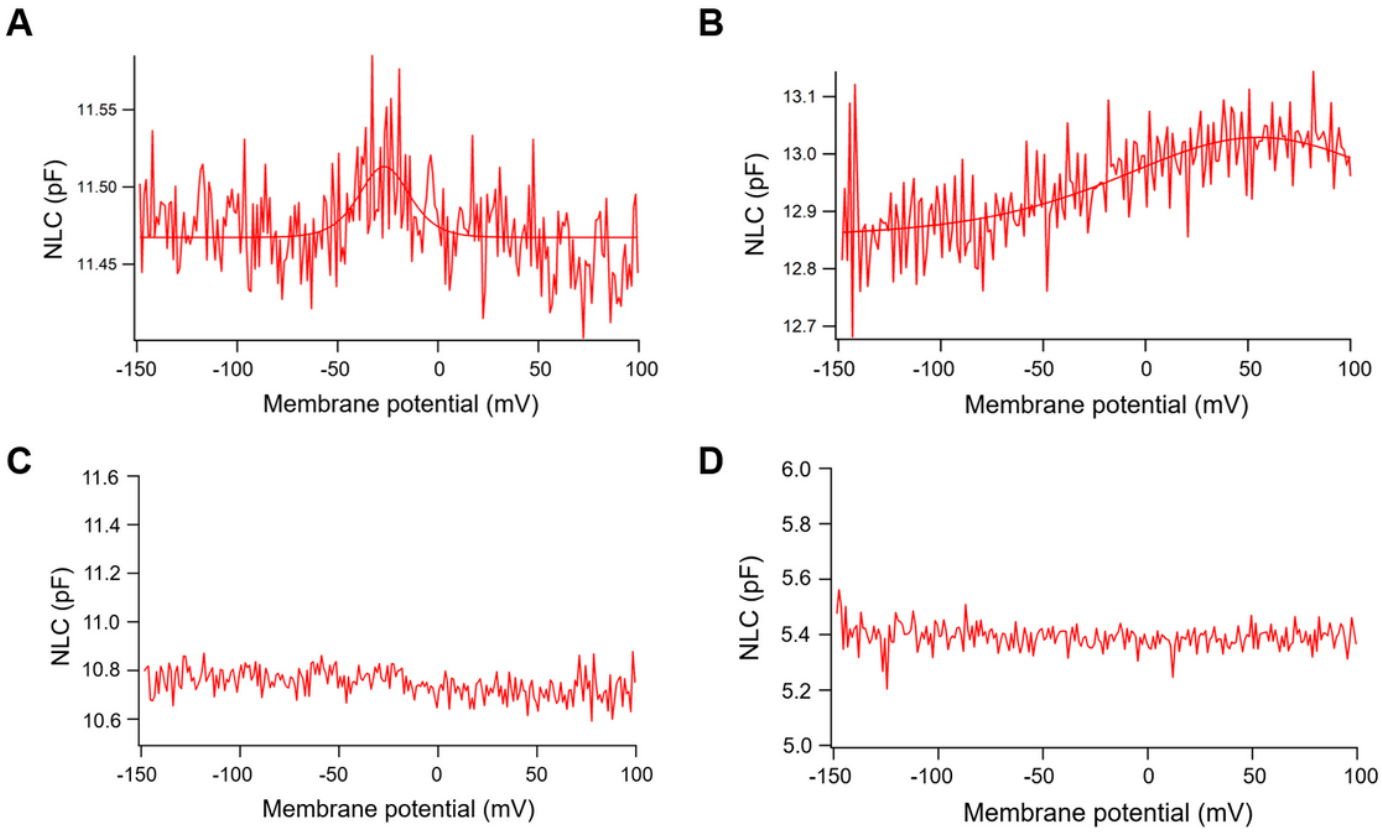

Figure 5

The nonlinear capacitance measurements of different species. A), Non-linear capacitance obtained from the HEK293T cells expressing bullfrog prestin. B), Non-linear capacitance obtained from the HEK293T cells expressing xenopus prestin. C), No NLC obtained from the HEK293T cells expressing chicken prestin. D), This one showed the lack of detectable NLC in a negative control cell.

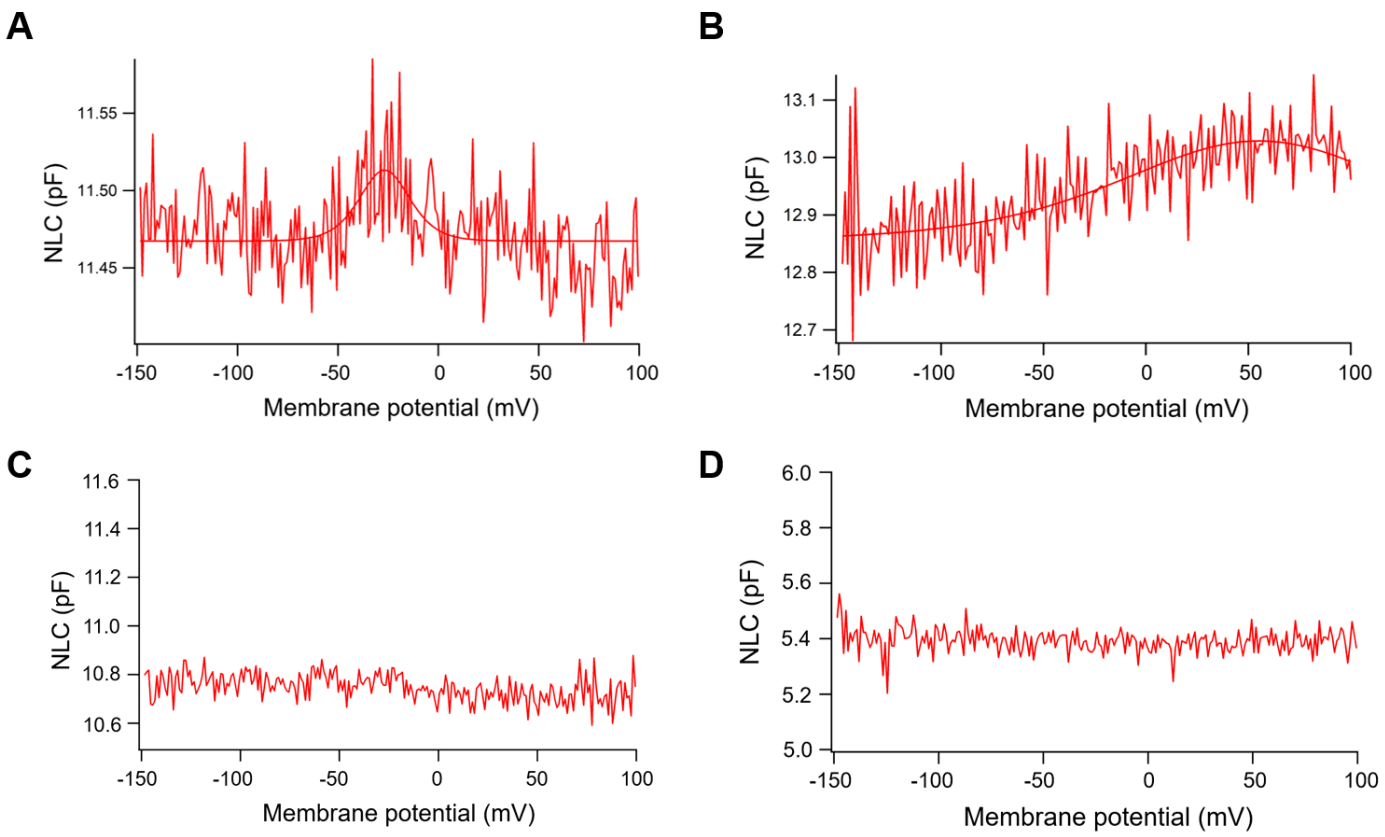

Figure 5

The nonlinear capacitance measurements of different species. A), Non-linear capacitance obtained from the HEK293T cells expressing bullfrog prestin. B), Non-linear capacitance obtained from the HEK293T cells expressing xenopus prestin. C), No NLC obtained from the HEK293T cells expressing chicken prestin. D), This one showed the lack of detectable NLC in a negative control cell.

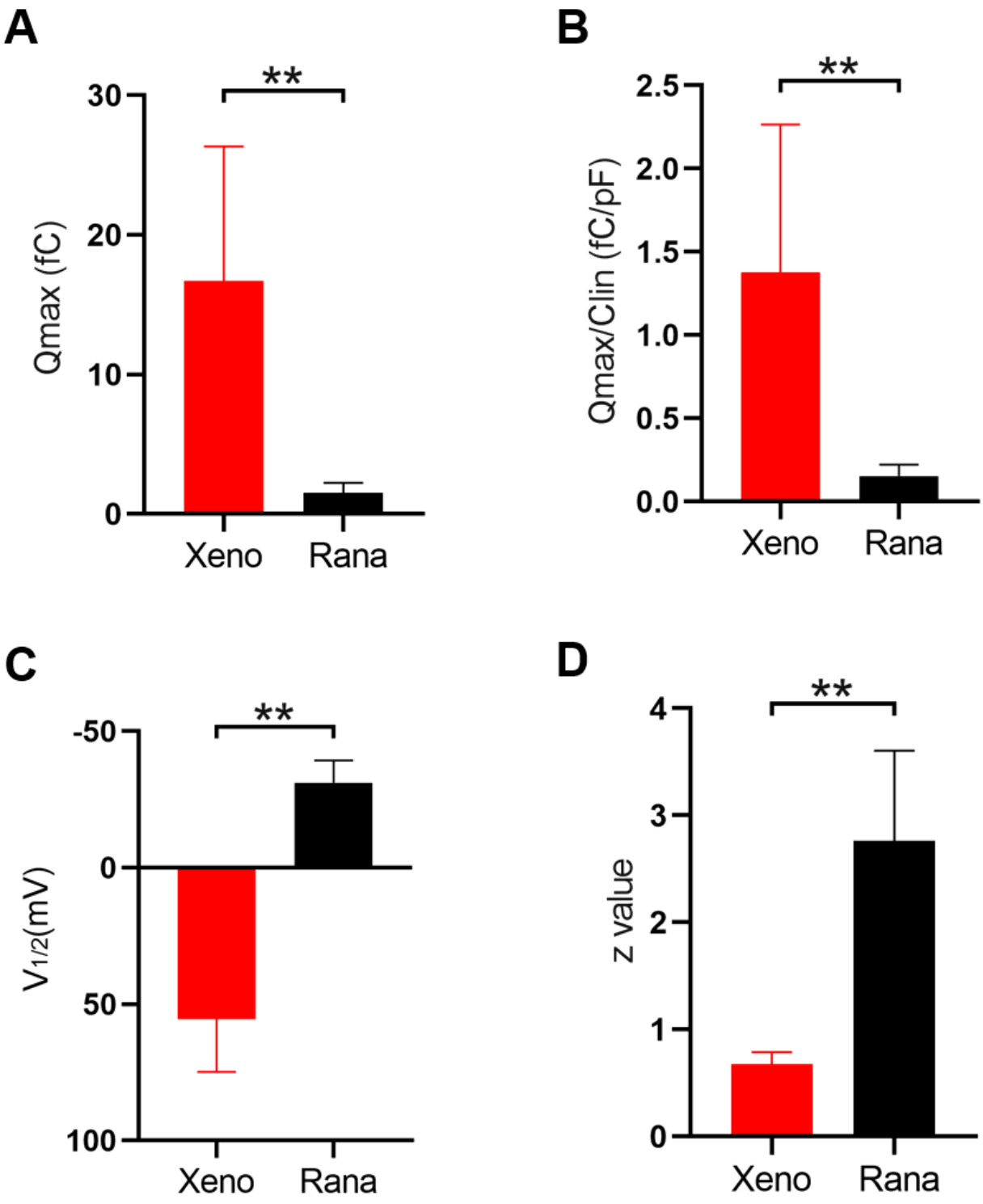

Figure 6

NLC datas of the HEK293T cells expressing xenopus prestin. A, B, C, D) Showed four parameters derived from curve fittings with Boltzmann's function for the cells (n=12). Datas were expressed as mean±s.d. *P < 0.05□**P < 0.01

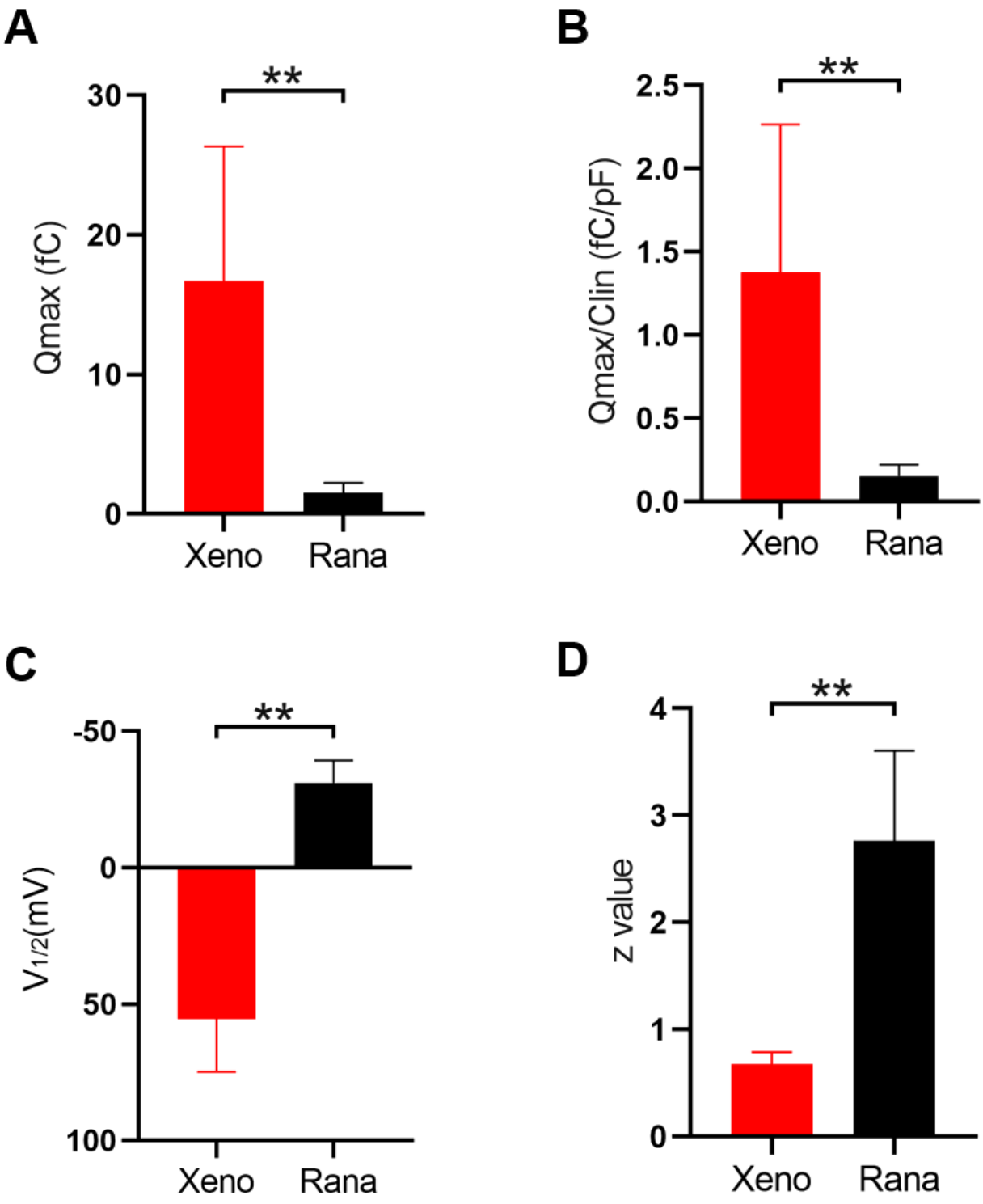

Figure 6

NLC datas of the HEK293T cells expressing xenopus prestin. A, B, C, D) Showed four parameters derived from curve fittings with Boltzmann's function for the cells (n=12). Datas were expressed as mean±s.d. *P < 0.05□**P < 0.01

Supplementary Files

This is a list of supplementary files associated with this preprint. Click to download.

- AuthorChecklistFull.pdf
- AuthorChecklistFull.pdf
- allthedatas.xlsx
- allthedatas.xlsx